downfield resonance at δ 2.42.[22] At 130 °C, there is presumably considerable conformational motion in the linker chain, such that the special metal–proton shielding interaction is averaged out. The integrated intensity of the broad upfield resonances (δ 1.61–1.32) corresponding to the remaining protons of the linker chain increases by the required amount at this higher temperature, indicating that protons (H_A) now resonate at a more normal frequency. The signals due to the geminal partners (H_B) are obscured in the upfield region of the proton spectrum at room temperature, preventing determination of the free energy of activation for this linker chain conformational rotation phenomenon.

(22) Villacorta, G. M.; Whang, E.; Lippard, S. J., unpublished results.

Acknowledgment. This work was supported by a grant from the National Science Foundation, Grant No. NSF CHE85-42205. We thank Dr. Dan Gibson for help in solving the crystal structure of *syn*-**1** and R. Lynn Rardin for computational assistance.

Registry No. *anti*-**1**, 111410-36-7; *syn*-**1**, 111467-16-4; $[Rh(CO)_2Cl]_2$, 14523-22-9.

Supplementary Material Available: Tables reporting heavy-atom thermal parameters (Tables S1 and S4) and hydrogen atom parameters (Tables S2 and S5) for *syn*-**1** and *anti*-**1** (4 pages); tables of observed and calculated structure factors (Tables S3 and S6) for *syn*-**1** and *anti*-**1** (25 pages). Ordering information is given on any current masthead page.

Contribution from the Department of Chemistry, Massachusetts Institute of Technology, Cambridge, Massachusetts 02139

Synthesis, Structure, and Characterization of the Tetranuclear Iron(III) Oxo Complex $[Fe_4O_2(BICOH)_2(BICO)_2(O_2CPh)_4]Cl_2$

Sergiu M. Gorun and Stephen J. Lippard*

Received August 31, 1987

The synthesis and characterization of a novel molecule containing the bis(μ_3-oxo)tetrairon(III) core, $[Fe_4O_2(BICOH)_2(BICO)_2(O_2CPh)_4]Cl_2$, where BICOH is bis(*N*-methylimidazol-2-yl)carbinol, are reported. Structural, magnetic, and Mössbauer studies indicate the presence of antiferromagnetically coupled iron(III) ions with a diamagnetic ground state. The $\{Fe_4O_2\}^{8+}$ core is formally comprised of two (μ-oxo)bis(μ-benzoato)diiron(III) centers, of the kind present in the marine invertebrate respiratory protein hemerythrin, joined by linkages between oxo ligands and iron atoms of the $\{Fe_2O\}^{4+}$ constituents. Additional bridges between the two $\{Fe_2O\}^{4+}$ components are provided by the $BICO^-$ ligands. The resulting tetranuclear complex has a planar Fe_2O_2 "kernel" with Fe–O bond lengths of 1.94 (1) and 1.98 (1) Å, Fe–O–Fe angles of 95.7 (5)°, and O–Fe–O angles of 84.3 (5)°. Within the $\{Fe_2O(O_2CPh)_2\}^{2+}$ subfragment the Fe–O bond lengths are 1.884 (9) Å and, shared with the kernel, 1.94 (1) Å, while the Fe–O–Fe angle is 119.0 (6)°. Similar $\{Fe_4O_2\}$ tetranuclear cores occur in the minerals amarantite and leucophosphite, as well as the recently reported discrete complex $[Fe_4O_2(O_2CCF_3)_8(H_2O)_6]$, the geometric properties of which are compared and analyzed. Optical spectroscopic features at ~465–475 and 565–575 nm are suggested to be characteristic of the $\{Fe_4O_2\}^{8+}$ unit. The coordinating properties of the biologically relevant bidentate BICOH ligand and its deprotonated, tridentate bridging $BICO^-$ derivative are described. X-ray studies were carried out on $[Fe_4O_2(BICOH)_2(BICO)_2(O_2CPh)_4]Cl_2 \cdot 5H_2O \cdot 2CH_3CN$, which crystallizes in the trigonal system, space group $R\bar{3}$, with $a = b = 39.128$ (8) Å, $c = 17.833$ (7) Å, $V = 23\,644$ Å^3, $Z = 9$, and $\rho_{calcd} = 1.106$ g cm^{-3}.

Introduction

Polynuclear oxo- or hydroxo-bridged iron(III) centers occur in a variety of proteins. Hemerythrin (Hr),[1] ribonucleotide reductase (RR)[2] and, probably, purple acid phosphatases (PAP)[3] contain binuclear units, while ferritins (Ft) and hemosiderins (Hs) have polynuclear units of uncertain size.[4] Planar tetranuclear oxo- and hydroxo-bridged iron(III) clusters also occur in nature in at least two minerals, amarantite, $[Fe_4O_2(SO_4)_4] \cdot 14H_2O$,[5] and leucophosphite, $K_2[Fe_4(OH)_2(PO_4)_4(H_2O)_2] \cdot 2H_2O$.[6] The FeO_6 octahedra in these minerals are arranged at the corners of a rhombus

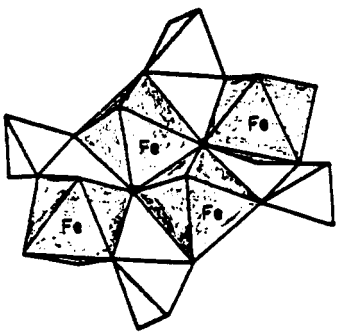

where the sulfate and phosphate anions are represented by tetrahedra. In leucophosphite there are two μ_3-OH units bridging the four iron atoms, while in amarantite their place is taken by two μ_3-oxo units. Both structures are polymeric.

Apart from the tetranuclear iron(III) complex (**1**) that forms the basis for this report, several related compounds have recently been synthesized. These include $[Fe_4O_2(O_2CCF_3)_8(H_2O)_6] \cdot 2H_2O$ (**2**),[7] $(Et_4N)[Fe_4O_2(O_2CPh)_7(H_2B(pz)_2)_2]$ (**3**),[8] where $H_2B(pz)_2^-$ is the dihydrobis(1-pyrazolyl)borate anion, $Na_6[Fe_4L_2O_2(CO_3)_2]$ (**4**),[9] where L is the pentaanionic form of [(2-hydroxy-1,3-

(1) (a) Klotz, I. M.; Kurtz, D. M., Jr. *Acc. Chem. Res.* **1984**, *17*, 16–22 and references therein. (b) Hendrickson, W. A. In *Invertebrate Oxygen-Binding Proteins: Structure, Active Site and Function*; Lamy, J., Lamy, J., Eds.; Marcel Dekker: New York, 1981; pp 503–515. (c) Stenkamp, R. E.; Sieker, L. C.; Jensen, L. H. *J. Am. Chem. Soc.* **1984**, *106*, 618–622 and references cited therein.

(2) (a) Reichard, P.; Ehrenberg, A. *Science* **1983**, *221*, 514–519 and references therein. (b) Sjöberg, B.-M.; Gräslund, A. *Adv. Inorg. Biochem.* **1983**, *5*, 87–110 and references therein.

(3) (a) Davis, J. C.; Averill, B. A. *Proc. Natl. Acad. Sci. U.S.A.* **1982**, *79*, 4623–4627. (b) Sinn, E.; O'Connor, C. J.; de Jersey, J.; Zerner, B. *Inorg. Chim. Acta.* **1983**, *78*, L13–L15. (c) Antanaitis, B. C.; Aisen, P.; Lilienthal, H. R. *J. Biol. Chem.* **1983**, *258*, 3166–3172. (d) Averill, B. A.; Davis, J. C.; Burman, S.; Zirino, T.; Sanders-Loehr, J.; Loehr, T. M.; Sage, J. T.; Debrunner, P. G. *J. Am. Chem. Soc.* **1987**, *109*, 3760–3767.

(4) (a) Ford, G. C.; Harrison, P. M.; Rice, D. W.; Smith, J. M. A.; Treffry, A.; White, J. L.; Yariv, J. *Philos. Trans. R. Soc. London, B* **1984**, *304*, 551–565. (b) Ford, G. C.; Harrison, P. M.; Rice, D. W.; Smith, J. M. A.; Treffry, A.; White, J. L.; Yariv, J. *Rev. Port. Quim.* **1985**, *27*, 119–120. (c) Spiro, T. G.; Saltman, P. *Struct. Bonding (Berlin)* **1969**, *6*, 116–156. (d) Spiro, T. G.; Pope, L.; Saltman, P. *J. Am. Chem. Soc.* **1967**, *89*, 5555–5559. (e) Spiro, T. G.; Bates, G.; Saltman, P. *J. Am. Chem. Soc.* **1967**, *89*, 5559–5562. (f) Theil, E. C. *Adv. Inorg. Biochem.* **1983**, *5*, 1–38 and references cited therein. (g) Fischbach, F. A.; Anderegg, J. W. *J. Mol. Biol.* **1965**, *14*, 458–473. (h) Smith, J. M. A.; Helliwell, J. R. *Inorg. Chim. Acta* **1985**, *106*, 193–196. (i) Mann, S.; Bannister, J. V.; Williams, R. J. P. *J. Mol. Biol.* **1986**, *188*, 225–232.

(5) Susse, P. *Z. Kristallogr.* **1968**, *127*, 261–275.

(6) Moore, P. B. *Am. Mineral.* **1972**, *57*, 397–410.

(7) Ponomarev, V. I.; Atovmyan, L. O.; Bobkova, S. A.; Turtê, K. I. *Dokl. Akad. Nauk. SSSR* **1984**, *274*, 368–372.

(8) Armstrong, W. H.; Roth, M. E.; Lippard, S. J., *J. Am. Chem. Soc.* **1987**, *109*, 6318–6326.

0020-1669/88/1327-0149$01.50/0

propanediyl)diimino]tetraacetic acid, and $Q_4[Fe_4O_2L_2(OH)_2]$ (**5**),[10] where Q is pyrrolidinium and HL is *N,N'*-(2-hydroxy-5-methyl-1,3-xylylene)bis(*N*-(carboxymethyl)glycine). The tetranuclear $\{Fe_4O_2\}^{8+}$ unit in **2** and **4** is planar or nearly planar, is considerably distorted from planarity in **3**, and forms part of a distorted tetrahedral array in **5**. The tetranuclear complex $[Fe_2O(O_2CCH_3)_2L_2]_2(NO_3)_4\cdot 4H_2O$ (**6**),[11] where L is tetrakis(2-pyridylmethyl)-1,4-butanediamine, does not contain the $\{Fe_4O_2\}^{8+}$ core but, rather, contains two isolated $\{Fe_2O\}^{4+}$ units. Tetranuclear halo methoxo,[12] methoxo alkanoato,[13,14] and pentanuclear carboxylato complexes[14] have been suggested in the literature, but structural information is lacking. Finally, the $\{Fe_4O_2\}^{8+}$ unit is present in the structure of the octairon complex $[Fe_8O_2(OH)_{12}(TACN)_6]Br_8\cdot 9H_2O$ (**7**),[15] where TACN = 1,4,7-triazacyclononane.

The present study was undertaken as part of ongoing efforts[16,17] in our laboratory to obtain functional models for Hr, the active site structure and oxygen-binding reaction for which are depicted in eq 1.[1,18,19] Benzoate anions were chosen to mimic the carboxylate moieties of the aspartic and glutamic acid residues present in the protein, and to replace the histidine residues, the potentially facially coordinating ligand bis(*N*-methylimidazol-2-yl)carbinol (BICOH) was selected. This ligand can be either tridentate, using

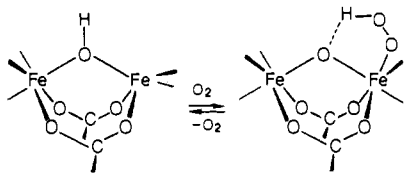

deoxyhemerythrin oxyhemerythrin (1)

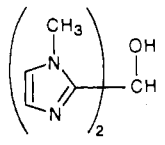

BICOH

NNO atoms, or bidentate, using either NN or NO atoms. The bidentate coordination mode would leave open coordination sites at the metal centers, facilitating reactions such as that given in eq 1. The choice of O over N donor atoms insures a greater thermodynamic stability of the resulting Fe(III) complex and promotes the formation of a high-spin complex by lowering the ligand-field strength at the metal sites, as demonstrated previously.[20]

As described in this report, attempts to assemble the hemerythrin model complex $[Fe_2O(O_2CPh)_2(BICOH)_2]^{2+}$ led instead to tetranuclear $[Fe_4O_2(BICOH)_2(BICO)_2(O_2CPh)_4]Cl_2$ (**1**). The chemistry reported here provides valuable insights, some of which were reinforced in parallel work in our laboratory on compound **3**,[8] into planning the synthesis of functional Hr analogues.

Table I. Details of the X-ray Crystallographic Study of $[Fe_4O_2(BICOH)_2(BICO)_2(O_2CPh)_4]Cl_2\cdot 5H_2O\cdot 2CH_3CN$[a]

formula	$Fe_4C_{68}H_{82}Cl_2N_{18}O_{19}$
fw	1749.81
space group	$R\bar{3}$
a, Å	39.128(8)
c, Å	17.833(7)
V, Å^3	23644.5
Z	9
ρ_{calcd}, g cm^{-3}	1.106
radiation	Mo Kα (0.71073 Å)
abs coeff, cm^{-1}	6.47
data collcd, deg	$3 \leq 2\theta \leq 50$
tot. no. of data collcd	10305
average, R_{av}	0.021
tot. no. of unique data	9227
no. of unique data with $I > 3\sigma(I)$	3761
no. of variable params	411
R_1[b]	0.0817
R_2[b]	0.1169

[a] Measurements were made at room temperature on an Enraf-Nonius CAD-4F κ-geometry diffractometer. [b] $R_1 = \sum||F_o| - |F_c||/\sum|F_o|$; $R_2 = [\sum w(|F_o| - |F_c|)^2/\sum w|F_o|^2]^{1/2}$.

Experimental Section

Preparation of Compounds. Solvents and reagents were obtained from commercial sources and used without further purification unless otherwise stated. $CHCl_3$, CH_3CN, and hexane were dried by distillation over P_4O_{10}, CaH_2, and sodium, respectively. Et_3N was distilled from phenyl isocyanate and stored over KOH under nitrogen. $(Et_4N)_2[Fe_2OCl_6]$,[21] was prepared by a literature method. BICOH was also prepared by a literature procedure[22] with the following modification. The crude reaction mixture was not extracted with ethyl acetate, but the solvents were removed in vacuo. The resulting solid was washed with acetone in order to remove unreacted starting materials. BICOH is only slightly soluble in acetone. The crude product was dissolved in hot CH_3CN, filtered, and recrystallized. The yield was only ~60% of the reported value, but the reaction was scaled up 10-fold and the total preparation time shortened by one-third. The spectroscopic properties of the white needles obtained were identical with the published ones. The chemical shift of the hydroxyl proton, which was not reported, was found to be 5.10 ppm in $CDCl_3$. Elemental analyses were performed by Atlantic Microlab, Inc., Atlanta, GA.

$[Fe_4O_2(BICOH)_2(BICO)_2(O_2CPh)_4]Cl_2\cdot 5H_2O\cdot 2CH_3CN$ ($1\cdot 5H_2O\cdot 2CH_3CN$). To a clear solution containing 0.387 g (6.44×10^{-4} mol) of $(Et_4N)_2[Fe_2OCl_6]$ in 6.5 mL of CH_3CN was added 0.186 g (1.29×10^{-3} mol) of anhydrous sodium benzoate while the mixture was being stirred rapidly for 0.5 h. In a separate flask, 0.247 g (1.29×10^{-3} mol) of BICOH was suspended in a mixture of 15 mL of CH_3CN and 5 mL of CH_2Cl_2. A 0.18-mL (1.3×10^{-3} mol) portion of Et_3N was added and, after being stirred for 1 h, the suspension was poured into the iron-containing solution. The resulting mixture was stirred for an additional hour and then filtered. The solvents were removed in vacuo and the solid was washed with 5 mL of a 35:65 (v:v) hexane:chloroform mixture. The dark green oil that resulted was washed three additional times with 5 mL of the above solvent mixture and dried under vacuum overnight to yield 0.32 g of a green solid. The solid was dissolved in 65 mL of warm CH_3CN. From the resulting green-yellow solution, crystals were obtained in any of three ways.

The first involved liquid–liquid diffusion, in which the solution was carefully layered on top of an equal volume of toluene. The toluene was not dried prior to use and contained ~0.03% H_2O, as reported by the manufacturer. The second method employed vapor–vapor diffusion by slowly evaporating the solution in an atmosphere saturated with water vapor. In the third approach, liquid–liquid diffusion was carried out as before, but the container was placed in an atmosphere saturated with water vapor, as in method 2. In all three cases, crystalline blocks were obtained in about 1 week, but the first method also yielded needlelike

(9) Jameson, D. L.; Xie, C.-L.; Hendrickson, D. N.; Potenza, J. A.; Schugar, H. J. *J. Am. Chem. Soc.* **1987**, *109*, 740–746.
(10) Murch, B. P.; Boyle, P. D.; Que, L. *J. Am. Chem. Soc.* **1985**, *107*, 6728–6729.
(11) Toftlund, H.; Murray, K. S.; Zwack, P. R.; Taylor, L. F.; Anderson, O. P. *J. Chem. Soc., Chem. Commun.* **1986**, 191–193.
(12) Kakos, G. A.; Winter, G. *Aust. J. Chem.* **1969**, *22*, 97–107.
(13) Kokot, E.; Mockler, G. M.; Sefton, G. L. *Aust. J. Chem.* **1973**, *26*, 2105–2113.
(14) Cattesick, J.; Thornton, P. *J. Chem. Soc., Dalton Trans.* **1977**, 1420–1425.
(15) Wieghardt, K.; Hohl, K.; Jibril, I.; Huttner, G. *Angew. Chem., Int. Ed. Engl.* **1984**, *23*, 77–78.
(16) (a) Armstrong, W. H.; Lippard, S. J. *J. Am. Chem. Soc.* **1983**, *105*, 4837–4838. (b) Armstrong, W. H.; Spool, A.; Papaefthymiou, G. C.; Frankel, R. B.; Lippard, S. J. *J. Am. Chem. Soc.* **1984**, *106*, 3653–3667. (c) Wieghardt, K.; Pohl, K.; Gebert, W. *Angew. Chem., Int. Ed. Engl.* **1983**, *22*, 727. (d) Chaudhuri, P.; Wieghardt, K.; Nuber, B.; Weiss, J. *Angew. Chem., Int. Ed. Engl.* **1985**, *24*, 778–779.
(17) Hartman, J. R.; Rardin, R. L.; Chaudhuri, P.; Pohl, K.; Wieghardt, K.; Nuber, B.; Weiss, J.; Papaefthymiou, G. C.; Frankel, R. B.; Lippard, S. J. *J. Am. Chem. Soc.*, in press.
(18) Shiemke, A. K.; Loehr, T. M.; Sanders-Loehr, J. *J. Am. Chem. Soc.* **1984**, *106*, 4951–4956.
(19) Reem, R. C.; Solomon, E. I. *J. Am. Chem. Soc.* **1987**, *109*, 1216–1226.
(20) (a) Gorun, S. M.; Lippard, S. J. *J. Am. Chem. Soc.* **1985**, *107*, 4568–4570. (b) Gorun, S. M.; Papaefthymiou, G. C.; Frankel, R. B.; Lippard, S. J. *J. Am. Chem. Soc.* **1987**, *109*, 4244–4255.
(21) Armstrong, W. H.; Lippard, S. J. *Inorg. Chem.* **1985**, *24*, 981–982.
(22) Tang, C. C.; Davalian, D.; Huang, P.; Breslow, R. *J. Am. Chem. Soc.* **1978**, *100*, 3918–3922.

crystals. Adding extra water to the toluene used in the first method gave flocculent precipitates. The hygroscopic crystals were dried under vacuum for 2 h. Isolated yields of crystals ranged from 10% to 25%. Anal. Calcd for $Fe_4C_{64}H_{76}Cl_2N_{16}O_{19}$, $[Fe_4O_2(BICOH)_2(BICO)_2(O_2CPh)_4]Cl_2 \cdot 5H_2O$: C, 46.09; H, 4.59; N, 13.44; Cl, 4.25. Found: C, 45.98; H, 4.83; N, 13.28; Cl, 4.80. IR (KBr, cm^{-1}): 3400 (br, s), 3120 (w), 2940 (w), 1600 (s), 1560 (s), 1510 (s), 1405 (s), 1290 (s), 1175 (m), 1075 (m), 1035 (m), 1015 (m), 975 (s), 915 (s), 860 (m), 730 (s), 685 (w), 620 (w), 585 (w), 470 (m). UV–vis (CH_2Cl_2, nm): 273 (sh), 313 (sh), 359 (sh), 373 (sh), 476 (sh), 575 (sh).

Collection and Reduction of X-ray Data. Dark red crystalline blocks large enough for X-ray diffraction studies were obtained by the slow diffusion processes described above over a period of 1–2 weeks. The crystals lose acetonitrile solvent readily and were sealed in glass capillaries containing a drop of mother liquor to avoid this problem. A block with approximate dimensions 0.43 × 0.40 × 0.51 mm was used for data collection. A linear decay in the intensity of standard reflections to 96.5% of the original values was observed and a correction applied. Owing to the low value (6.5 cm^{-1}) of the linear absorption coefficient, the fairly uniform crystal shape, and the difficulty of measuring and indexing the faces of crystals immersed in their mother liquor, no absorption correction was applied. The unit cell parameters and a systematic check for higher symmetry space groups[23] indicated that the crystal belongs to the rhombohedral system. Structure factor relationships were used to eliminate space groups having $\bar{3}m$ Laue symmetry. A supplementary check failed to reveal any glide planes. The final choice between space groups $R3$ (C_3^4, No. 146)[24a] and $R\bar{3}$ (C_{3i}^2, No. 148)[24b] was made on the basis of a statistical Debye–Wilson analysis, which suggested the centric space group $R\bar{3}$. This choice was confirmed by the successful solution and refinement of the structure. Further details concerning data collection and reduction can be found in ref 25 and Table I.

Structure Solution and Refinement. Iron atom positions were determined by direct methods.[26] The molecule sits on an inversion center at $^1/_2$, 0, $^1/_2$. All remaining non-hydrogen atoms were located from difference Fourier maps. In order to reduce the number of variables, the phenyl rings of the benzoate residues were constrained to regular hexagons and hydrogen atoms were placed at calculated positions. The C–C and C–H bonds were fixed at 1.395 Å and 0.95 Å, respectively, and the hydrogen atoms were allowed to "ride" on the carbon atoms to which they are attached. The positions of the imidazole hydrogen atoms were also calculated. One acetonitrile and two hydrogen-bonded water molecules are present per asymmetric unit. An additional non-hydrogen-bonded, crystallographically disordered water molecule with 0.5 site occupancy factor was located, bringing the total number of waters of crystallization to five, consistent with the elemental analysis. Acetonitrile molecules were not detected by elemental analysis, presumably because they were removed by drying in vacuo (vide supra). The first water molecule, O1W, is 2.7 Å from the alkoxo type oxygen O40, 2.8 Å from O2W, and ~3 Å from the hydroxo type oxygen, O10. The second water molecule, O2W, in addition to being hydrogen bonded to O1W, is 3 Å from Cl1, the latter being also 3.1 Å from the hydroxo oxygen, O10. Thus, O10, Cl1, O2W, and O1W form a quadrangle bonded to O40 through O1W. This hydrogen bond network provides supplementary linkages between the crystallographically related halves of the tetranuclear complex.

Least-squares refinement using the program SHELX-76[27] and minimizing the function $\sum w(|F_o| - |F_c|)^2$ converged to the R values listed in Table I. Neutral-atom scattering factors and anomalous dispersion corrections for the non-hydrogen atoms, as well as hydrogen atom scattering factors, were obtained from the sources quoted in ref 25. Anisotropic thermal parameters were assigned to all non-hydrogen atoms with the exception of the phenyl carbon atoms and the acetonitrile groups. Use of isotropic temperature factors for these latter atoms resulted in an important saving in the number of variable parameters. The largest residual peak in the final difference map was 0.72 e $Å^{-3}$, located on an inversion center and not connected directly to the rest of the molecule. All the site occupancy factors (SOF) and thermal parameters of the solvent molecules were allowed initially to vary. With the exception of the third water molecule, which gives an SOF value close to 0.5, full occupancy was reached for the solvent molecules. Consequently, the SOF's were fixed at 1.0 (0.5 for O3W) and only the thermal parameters were varied. Attempts to model the residual electron density as disordered water, acetonitrile, or toluene failed, but the low value of the calculated crystal density supports the presence of additional solvent in the lattice. An accurate value for the density could not be obtained experimentally.

Positional parameters for non-hydrogen atoms are presented in Table II; in the supplementary material, thermal parameters are given in Table S1, positional and thermal parameters for hydrogen atoms are given in Table S2, and a list of observed and calculated structure factors is given in Table S3.

Table II. Final Positional Parameters for Non-Hydrogen Atoms of $[Fe_4O_2(BICO)_2(BICOH)_2(O_2CPh)_4]Cl_2 \cdot 2CH_3CN \cdot 5H_2O$[a,b]

atom	x	y	z
Fe1	0.57880 (10)	0.05130 (10)	0.58710 (10)
Fe2	0.50990 (10)	0.03720 (10)	0.46460 (10)
O	0.5362 (3)	0.0164 (3)	0.5261 (5)
O1	0.4958 (3)	0.0602 (3)	0.5520 (6)
O2	0.5528 (3)	0.0841 (3)	0.6152 (6)
O3	0.6075 (3)	0.0898 (3)	0.4983 (6)
O4	0.5569 (3)	0.0930 (3)	0.4474 (6)
O10	0.6683 (4)	0.0460 (4)	0.7170 (8)
O40	0.5661 (3)	0.0260 (3)	0.6840 (5)
C10	0.6734 (6)	0.0630 (6)	0.6481 (11)
N11	0.6573 (4)	0.0056 (4)	0.5648 (8)
C12	0.6472 (5)	0.0316 (5)	0.5917 (9)
N13	0.6148 (3)	0.0265 (4)	0.5585 (7)
C14	0.6035 (5)	−0.0042 (5)	0.5093 (9)
C15	0.6299 (5)	−0.0170 (5)	0.5129 (10)
C16	0.6913 (6)	0.0005 (6)	0.5882 (12)
N21	0.6944 (5)	0.1318 (5)	0.6743 (10)
C22	0.6658 (5)	0.0962 (5)	0.6536 (10)
N23	0.6321 (4)	0.0966 (4)	0.6395 (7)
C24	0.6403 (5)	0.1343 (5)	0.6528 (10)
C25	0.6789 (6)	0.1548 (6)	0.6755 (12)
C26	0.7351 (6)	0.1440 (7)	0.6927 (17)
N31	0.5215 (4)	0.0039 (4)	0.2454 (8)
C32	0.5042 (5)	0.0137 (5)	0.3000 (9)
N33	0.5261 (4)	0.0236 (4)	0.3600 (7)
C34	0.5591 (5)	0.0212 (5)	0.3421 (10)
C35	0.5563 (5)	0.0091 (6)	0.2712 (10)
C36	0.5055 (5)	0.9883 (7)	0.1710 (10)
C40	0.4646 (5)	0.0111 (5)	0.2909 (9)
N41	0.4447 (4)	0.0633 (4)	0.3067 (9)
C42	0.4634 (4)	0.0441 (5)	0.3323 (9)
N43	0.4792 (4)	0.0587 (4)	0.3987 (7)
C44	0.4706 (5)	0.0877 (5)	0.4155 (10)
C45	0.4501 (6)	0.0905 (6)	0.3599 (12)
C46	0.4229 (6)	0.0566 (6)	0.2359 (11)
C50	0.5189 (5)	0.0784 (5)	0.6063 (9)
C51	0.5021 (4)	0.0939 (4)	0.6632 (7)
C52	0.4658 (4)	0.0919 (4)	0.6532 (7)
C53	0.4506 (4)	0.1053 (4)	0.7095 (7)
C54	0.4718 (4)	0.1207 (4)	0.7758 (7)
C55	0.5081 (4)	0.1226 (4)	0.7858 (7)
C56	0.5232 (4)	0.1092 (4)	0.7295 (7)
C60	0.5934 (5)	0.1054 (5)	0.4574 (9)
C61	0.6217 (3)	0.1408 (3)	0.4178 (7)
C62	0.6610 (3)	0.1623 (3)	0.4404 (7)
C63	0.6877 (3)	0.1958 (3)	0.4005 (7)
C64	0.6750 (3)	0.2078 (3)	0.3379 (7)
C65	0.6356 (3)	0.1863 (3)	0.3153 (7)
C66	0.6090 (3)	0.1528 (3)	0.3553 (7)
Cl1	0.4195 (2)	0.3975 (2)	0.0831 (4)
O1W	0.6097 (5)	0.0572 (6)	0.8075 (9)
O2W	0.5690 (7)	0.0109 (9)	0.9300 (16)
O3W	0.1347 (16)	0.040 (2)	0.225 (3)
N1S	0.4287 (10)	0.2298 (10)	0.4961 (18)
C2S	0.4337 (12)	0.2031 (14)	0.501 (2)

[a] Atoms are labeled as shown in Figures 1 and 2. Atomic positional coordinates x', y', and z' of the second, symmetry-related half of the complex are related to the listed coordinates, x, y, z, by the relationships $x' = 0.5 - x$, $y' = -y$, and $z' = 0.5 - z$. The two phenyl rings were numbered cyclically, starting with Cn1 to which the carboxylic Cn0 atom is attached. The two rings have $n = 5$ and 6. [b] Numbers in parentheses are errors in the last significant digit(s).

(23) Lawton, S. L. "Tracer II, A Fortran Lattice Transformation-Cell Reduction Program"; Mobil Oil Corp.: Paulsboro, NJ; 1978.

(24) *International Tables for Crystallography*; Hahn, T., Ed.; D. Reidel: Dordrecht, The Netherlands, and Boston, MA, 1983; Volume A: (a) p 484; (b) p 490.

(25) Silverman, L. D.; Dewan, J. C.; Giandomenico, C. M.; Lippard, S. J. *Inorg. Chem.* **1980**, *19*, 3379-3383, and references therein.

(26) Germain, G.; Main, P.; Woolfson, M. M. *Acta Crystallogr., Sect. A*: **1971**, *A27*, 368–376.

(27) SHELX-76: Sheldrick, G. M. In *Computing in Crystallography*; Schenk, H., Olthoff-Hazekamp, R., Van Koningsveld, H., Bassi, G. C., Eds.; Delft University Press: Delft, The Netherlands, 1978; pp 34–42.

Magnetic Measurements. Two sets of data were recorded and processed by following the procedures described elsewhere.[20] Solvated crystalline samples were powdered under N_2 and dried under vacuum for 2 h at room temperature. In this manner, all of the solvated acetonitrile was removed. Variable-temperature magnetic susceptibility measurements were carried out with an S.H.E. Model 905 SQUID-type susceptometer at 20 kOe. The low-temperature molar susceptibilities were analyzed by using the Curie–Weiss law.

Infrared and Optical Spectroscopy. Infrared spectra in the range 4000–400 cm^{-1} were recorded with a Beckman Acculab 10 instrument at 5 cm^{-1} accuracy. Electronic spectra in the range 220–800 nm were recorded with Perkin–Elmer Lambda 7 and Cary Model 118C spectrophotometers. The accuracy in position of the shoulders is 5 nm.

Mössbauer Spectroscopy. Mössbauer spectra of powdered samples were recorded at 4.2 K at 0 and 60 kOe longitudinal applied fields. The isomer shifts were measured relative to that of iron metal at room temperature.

Results and Discussion

Synthesis. The chemical reaction proposed for the synthesis of **1** is given by eq 2. Triethylamine was added to facilitate removal of the proton and formation of the alkoxide moiety of

$$(Et_4N)_2[Fe_2OCl_6] + 2Na(O_2CPh) + 2BICOH \xrightarrow[Et_3N]{CH_3CN} {}^1/_2[Fe_4O_2(BICOH)_2(BICO)_2(O_2CPh)_4]Cl_2 + 2NaCl + 2Et_4NCl + Et_3NHCl \quad (2)$$

the $BICO^-$ anion. The stoichiometry is correct for obtaining a (μ-oxo)bis(μ-carboxylato)diiron(III) core in which the terminal facial positions are occupied by two imidazole nitrogen atoms and the alkoxide oxygen atom. Instead of this Hr type structure, however, a tetranuclear product forms in which, formally at least, two $\{Fe_2O\}^{4+}$ cores have associated, as depicted by eq 3.

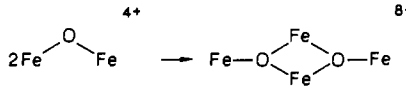

(3)

A yellow solid obtained along with the dark red crystals of **1** can be separated mechanically by suspending the mixture in mother liquor and removing the majority of the turbid liquid phase. The procedure can be repeated until the liquid phase is clear. The yellow solid was not identified, but its infrared spectrum suggested that it could be a hydroxo complex, formed from adventitious water present in the reaction mixture. Iron(III) complexes containing hydroxo groups and various ligands are well-known.[16,28] Crystals of **1** are stable when stored under solvent. Some water is necessary in order to obtain crystalline, solvated products, but too much water or use of higher concentrations or faster diffusion rates during the synthesis leads to hydrolysis. A blue complex, which was not isolated, but was tentatively identified spectroscopically as $[Fe(BIK)_3]^{2+}$, where BIK is bis(*N*-methylimidazol-2-yl) ketone, is among the products.[20b] The formation of this complex is not unreasonable, since the ligand BICOH could be oxidized to the corresponding ketone in the presence of water, oxygen, and/or Fe^{3+}, as represented by eq 4, where R is *N*-

$$\underset{\text{BICOH}}{R_2CHOH} \xrightarrow{Fe^{3+}} \underset{\text{BIK}}{R_2C{=}O} \xrightarrow{Fe^{2+}} [Fe(BIK)_3]^{2+} \quad (4)$$

methylimidazol-2-yl. Oxidation of 1,1,2-tris(*N*-methylimidazol-2-yl)-1-hydroxyethane (TIEOH) by Fe(III) and oxygen to form $[Fe(BIK)_3]^{2+}$ in a similar reaction was noted previously.[20]

Tetranuclear Fe(III) clusters have now been obtained by a variety of synthetic procedures. In the first method,[7] iron redox chemistry plays an important, but as yet unelucidated, role. Formation of $[Fe_4O_2(O_2CCF_3)_8(H_2O)_6]\cdot 2H_2O$ (**2**) is accomplished by slow evaporation in air of a solution of the trinuclear mixed-valence complex $[Fe_3O(O_2CCF_3)_6(H_2O)_3]$.[29] The composition and oxidation state of iron in **2** were established by X-ray diffraction and Mössbauer studies.[30] A second method, employed for **5**, involves dimerization of the preformed binuclear complex $[Fe_2L(OH)(H_2O)_2]$ in aqueous base.[10] This binuclear complex presents three potential deprotonation sites: two water molecules coordinated to Fe and one bridging hydroxide group. The ligand provides an additional bridging phenoxide and two terminal carboxylate groups, as well as nitrogen atoms to cap each iron center. Formally, during one dimerization reaction, the metal-bound water molecules are displaced, μ-hydroxide bridges are broken, and two new μ-hydroxo and μ-oxo bridges are formed. The structural formula of the core is $\{Fe_4(\mu\text{-}O)_2(\mu\text{-}OH)_2(\mu\text{-}OL)_2\}^{4-}$, where LO^- symbolizes the phenoxide moiety of L. The four iron atoms constitute a tetrahedral core. A third method, employed in the synthesis of the bis-dinuclear complex **6**, starts with the classic trinuclear basic iron acetate and ligand in aqueous ethanol.[11] A fourth method, used to prepare **4**, employs $Fe(OH)_3$, ligand, and $NaHCO_3$ in water.[9] Finally, in the syntheses of **1** and **3**,[8] the preformed (μ-oxo)diiron(III) compound $(Et_4N)_2[Fe_2OCl_6]$ is used as the source of iron. The same starting material was employed to prepare the asymmetric $\{Fe_3O\}^{7+}$ core described previously.[20] The variety of routes to tetranuclear iron(III) is consistent with the notion that the reactions are under thermo-

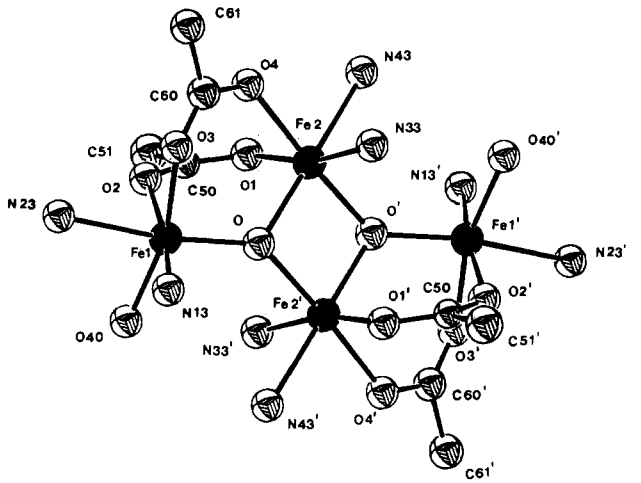

Figure 1. Drawing of the $\{Fe_4O_2\}^{8+}$ inner core geometry of **1**, showing the 40% probability thermal ellipsoids and atom labels. Only the first carbon atoms of the phenyl rings are depicted.

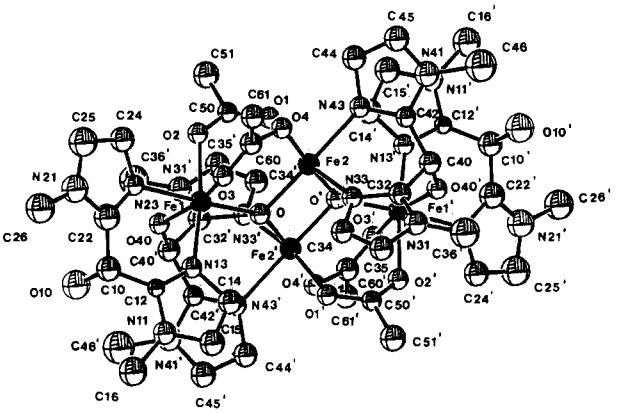

Figure 2. Full drawing of the $[Fe_4O_2(BICOH)_2(BICO)_2(O_2CPh)_4]^{2+}$ cation in **1**, showing the 40% probability thermal ellipsoids and labels for all non-hydrogen atoms. Only the first carbon atoms of the phenyl rings are presented.

(28) (a) Thich, J. A.; Ou, C. C.; Powers, D.; Vasiliou, B.; Mastropaolo, D.; Potenza, J. A.; Schugar, H. J. *J. Am. Chem. Soc.* **1976**, *98*, 1425–1433. (b) Ou, C. C.; Lalancette, R. A.; Potenza, J. A.; Schugar, H. J. *J. Am. Chem. Soc.* **1978**, *100*, 2053–2057. (c) Chiari, B.; Piovesano, O.; Tarantelli, T.; Zanazzi, P. F. *Inorg. Chem.* **1983**, *22*, 2781–2784. (d) Armstrong, W. H.; Lippard, S. J. *J. Am. Chem. Soc.* **1984**, *106*, 4632–4633.

(29) Ponomarev, V. I.; Filipenko, O. S.; Atovmyan, L. O. *Dokl. Akad. Nauk SSSR* **1982**, *262*, 346–349.

(30) Stukan, R. A.; Ponomarev, V. I.; Nifontov, V. P.; Turtê, K. I.; Atovmyan, L. O. *Zh. Strukt. Khim.* **1985**, *26*, 62–66.

Table III. Interatomic Distances (Å) and Angles (deg) for $[Fe_4O_2(BICO)_2(BICOH)_2(O_2CPh)_4]Cl_2 \cdot 2CH_3CN \cdot 5H_2O$[a]

		Iron Coordination Spheres			
Fe1–O	1.884 (9)	Fe1–O40	1.929 (9)	Fe1–O2	2.06 (1)
Fe1–O3	2.08 (1)	Fe1–N13	2.13 (2)	Fe1–N23	2.16 (1)
Fe2–O	1.94 (1)	Fe2–O′	1.974 (9)	Fe2–O1	2.01 (1)
Fe2–O4	2.056 (9)	Fe2–N33	2.12 (1)	Fe2–N43	2.13 (2)
O–Fe1–O40	103.8 (4)	O–Fe1–O2	93.4 (5)	O–Fe1–O3	92.7 (4)
O–Fe1–N13	94.5 (5)	O–Fe1–N23	170.2 (4)	O40–Fe1–O2	91.2 (5)
O40–Fe1–O3	163.5 (4)	O40–Fe1–N13	92.3 (6)	O40–Fe1–N23	85.9 (4)
O2–Fe1–O3	89.4 (5)	O2–Fe1–N13	170.4 (4)	O2–Fe1–N23	87.6 (6)
O3–Fe1–N13	84.7 (5)	O3–Fe1–N23	77.6 (4)	N13–Fe1–N23	83.7 (6)
O–Fe2–O′	84.3 (5)	O–Fe2–O1	94.1 (5)	O–Fe2–O4	98.6 (5)
O–Fe2–N33	96.0 (6)	O–Fe2–N43	178.1 (4)	O′–Fe2–O1	95.8 (4)
O′–Fe2–O4	176.1 (4)	O′–Fe2–N33	92.1 (4)	O′–Fe2–N43	94.0 (5)
O1–Fe2–O4	86.6 (4)	O1–Fe2–N33	167.8 (6)	O1–Fe2–N43	85.2 (6)
O4–Fe2–N33	85.1 (5)	O4–Fe2–N43	83.1 (5)	N33–Fe2–N43	85.0 (6)
Fe1–O–Fe2	119.0 (6)	Fe1–O–Fe2′	136.8 (6)	Fe2–O–Fe2′	95.7 (5)
		Carboxylate Geometries			
O1–C50	1.27 (2)	O2–C50	1.24 (2)	O3–C60	1.24 (3)
O4–C60	1.27 (2)	C50–C51	1.49 (3)	C60–C61	1.45 (2)
C50–O1–Fe2	124 (1)	C50–O2–Fe1	132 (1)	C60–O3–Fe1	126 (1)
C60–O4–Fe2	128 (1)				
O2–C50–O1	126 (2)	O2–C50–C51	119 (1)	O1–C50–C51	114 (2)
O3–C60–O4	126 (1)	O3–C60–C61	116 (1)	O4–C60–C61	118 (2)
		Ligand Geometries			
O10–C10	1.36 (2)	O40–C40	1.42 (2)		
C10–C22	1.47 (4)	C10–C12	1.52 (2)	N11–C12	1.35 (3)
N11–C15	1.36 (2)	N11–C16	1.50 (3)	C12–N13	1.32 (2)
N13–C14	1.37 (2)	C14–C15	1.36 (3)	N21–C25	1.31 (4)
N21–C22	1.33 (2)	N21–C26	1.45 (3)	C22–N23	1.35 (3)
N23–C24	1.36 (3)	C24–C25	1.37 (3)	C26–N21	1.45 (3)
N31–C32	1.35 (3)	N31–C35	1.35 (3)	N31–C36	1.46 (2)
C32–N33	1.30 (2)	C32–C40	1.51 (3)	N33–C34	1.38 (3)
C34–C35	1.34 (3)	C40–C42	1.51 (3)	N41–C45	1.36 (3)
N41–C42	1.36 (3)	N41–C46	1.47 (3)	C42–N43	1.33 (2)
N43–C44	1.37 (3)	C44–C45	1.31 (3)		
C12–N13–Fe1	129 (1)	C14–N13–Fe1	124 (1)	C24–N23–Fe1	125 (1)
C22–N23–Fe1	128 (1)	C32–N33–Fe2	124 (1)	C34–N33–Fe2	129 (1)
C42–N43–Fe2	124 (1)	C44–N43–Fe2	129 (1)		
C22–C10–C12	114 (2)	C12–N11–C15	107 (2)	C12–N11–C16	128 (1)
C15–N11–C16	125 (2)	N13–C12–N11	110 (1)	N13–C12–C10	129 (2)
N11–C12–C10	121 (2)	C12–N13–C14	107 (2)	C15–C14–N13	109 (1)
C14–C15–N11	107 (2)	C25–N21–C22	107 (2)	C25–N21–C26	125 (2)
C22–N21–C26	128 (2)	N21–C22–N23	111 (2)	N21–C22–C10	120 (2)
N23–C22–C10	129 (1)	C22–N23–C24	106 (1)	N23–C24–C25	106 (2)
N21–C25–C24	110 (2)	C32–N31–C35	109 (1)	C32–N31–C36	127 (2)
C35–N31–C36	124 (2)	N33–C32–N31	109 (2)	N33–C32–C40	127 (2)
N31–C32–C40	123 (1)	C32–N33–C34	107 (2)	C35–C34–N33	109 (2)
C34–C35–N31	106 (2)	C42–C40–C32	111 (1)	C45–N41–C42	106 (2)
C45–N41–C46	126 (2)	C42–N41–C46	128 (2)	N43–C42–N41	109 (2)
N43–C42–C40	127 (2)	N41–C42–C40	124 (1)	C42–N43–C44	107 (2)
C45–C44–N43	109 (2)	C44–C45–N41	109 (2)		
C40–O40–Fe1	132.7 (9)	O10–C10–C22	109 (2)	O10–C10–C12	109 (1)
O40–C40–C42	110 (1)	O40–C40–C32	111 (2)		
		Solvent Geometries			
N1S–C2S	1.16 (8)	C2S–C3S	1.47 (9)	N1S–C2S–C3S	179 (4)

[a] See footnotes *a* and *b*, Table II. Phenyl rings, constrained to regular hexagons, are omitted. O40 and O10 are the alkoxo and hydroxyl type oxygen atoms, respectively. C40 and C10 connect the imidazole rings numbered 1 and 2 and 3 and 4, respectively. X*nm* denotes the *m*th atom of the *n*th imidazole ring. S stands for solvent. The primed atoms are related to their unprimed counterparts by an inversion center.

dynamic, rather than kinetic, control.

Description of Structure. The structure of the tetranuclear cation in **1** can be formally viewed as a dimer of (μ-oxo)bis(μ-benzoato)diiron(III) units related by a crystallographically required inversion center, with imidazole nitrogen and alkoxide oxygen atoms of the $BICO^-$ and BICOH ligands completing octahedral coordination at each metal center (Figure 1). A more complete view of the structure is given in Figure 2, and a listing of interatomic distances and angles can be found in Table III. The four iron atoms lie at the corners of a rhombus, with Fe2 and Fe2′ defining the short diagonal and Fe1 and Fe1′ the long one. The two crystallographically independent iron atoms are bridged by two benzoate groups and by the μ_3-oxo atom, which links them to a third, symmetry-generated iron (Figure 2). Each iron is coordinated by two nitrogen atoms, from BICOH, in the case of the Fe1-type atoms, or from $BICO^-$ in the case of the "inner" iron, Fe2. Fe1, the "outer" iron, has as its sixth ligand O40, the deprotonated alkoxide oxygen belonging to the $BICO^-$ which binds to Fe2′ (Figure 3). There are two kinds of bis[*N*-methylimidazol-2-yl]carbinol ligands, BICOH which is bidentate and terminal, and $BICO^-$, which is tridentate and bridging. The two distinct octahedral coordination spheres can be summarized as

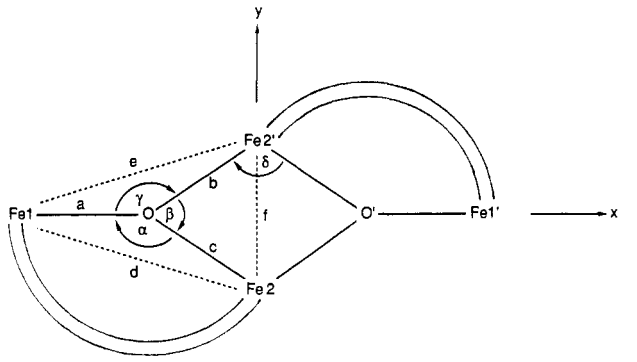

Figure 3. Diagram of the $\{Fe_4O_2\}$ core, defining its metrical parameters. Primed and unprimed atoms are related by an inversion center.

follows: Fe1, N_2O(alkoxide)$O(\mu_3$-oxo$)O_2$(benzoate); Fe2, $N_2O_2(\mu_3$-oxo$)O_2$(benzoate).

The Fe–N and Fe–O bond lengths are characteristic for high-spin ferric complexes (Table III). For binuclear μ-oxo complexes, the Fe–N distances range from 2.04 to 2.25 Å,[17,31,32] encompassing the average length of 2.14 Å found for **1**. This value compares favorably with the iron–imidazole nitrogen distances of 2.15 Å encountered in the trinuclear high-spin complex $[Fe_3O(TIEO)_2(O_2CPh)_2Cl_3]$ and in mononuclear high-spin [Fe(TIEO)(HTIEO)]$(ClO_4)_2$.[20] On the other hand, in low- or intermediate-spin mononuclear $[Fe(TICOH)_2]^{3+}$, the average Fe–N distance is 1.946 Å.[33] The difference is 0.19 Å, in accord with the value of 0.13 Å estimated as a lower limit for the difference between Fe–N bond lengths in high- and low-spin ferric complexes.[34] The average (⟨ ⟩) and range ([ ]) of Fe-O(μ_3-oxo) distances, ⟨1.935 Å⟩ and [1.88–1.98 Å], fall outside the [1.77–1.80 Å] range observed in (μ-oxo)bis(μ-carboxylato)diiron(III) complexes[17] but are close to the ⟨1.9 Å⟩ value known for the $\{Fe_3O\}^{7+}$ core in basic iron carboxylates.[35] In **1**, there are three independent Fe(III)–μ_3-oxo distances, all different from one another. This result may be contrasted with the geometries of the symmetric basic iron(III) carboxylates, where all three μ_3-oxo bridge bonds are equivalent, and of the asymmetric $\{Fe_3O\}$ complex $[Fe_3O(TIEO)_2(O_2CPh)_2Cl_3]$, where two of the three are equal.[20] The Fe–O(benzoate) bond lengths, ⟨2.05 Å⟩ and [2.01 (1)–2.08 (1) Å], are similar to the corresponding values found in $[Fe_3O(TIEO)_2(O_2CPh)_2Cl_3]$ (⟨2.058 Å⟩ and [2.034 (7)–2.080 (7) Å][20]) and in $[Fe_{11}O_6(OH)_6(O_2CPh)_{15}]\cdot 6THF$ (⟨2.042 Å⟩ and [1.967 (7)–2.106 (8) Å][35]). Within experimental error, there is no difference between Fe–N bond lengths Fe1–N23 and Fe2–N43 trans to the μ_3-oxo group and Fe1–N13 and Fe1–N33 cis to the oxo ligand. Such a difference occurs in (μ-oxo)bis(μ-carboxylato)diiron(III) complexes.[17] Angles for trans Fe–ligand bonds of the distorted iron octahedra range from 165.5 (O40–Fe1–O3) to 178.9° (O–Fe2–N43), while cis bond angles range from 77.6 (O3–Fe1–N23) to 103.8° (O-Fe1-O40). The ligand N–Fe–N "bite angles" are 85.0 (6) and 83.7 (6)°.

$\{Fe_2O_2\}$—A Structural Invariant in the $\{Fe_4O_2\}$ Core. A diagram of the $\{Fe_4O_2\}^{8+}$ core is presented in Figure 3, where the curved lines represent the bridging benzoate groups. Let us define "the dimer" to be the $\{Fe_2OL_n\}$ binuclear unit, where L denotes the ligands [e.g., L = (BICOH), (BICO), and benzoate groups in the case of compound **1**] and "the kernel" to be the {Fe2OFe2'O'} subset of atoms in the tetranuclear aggregate. Distances *a*–*e* and angles α–δ are defined to facilitate comparison of $\{Fe_4O_2\}$ units

Table IV. Metrical Parameters (in Å and deg) of Selected $\{Fe_4O_2\}^{n+}$ Type Cores with μ_3-O or μ_3-OH Bridges[a]

compd	core formula	α	β	γ	δ	*a*	*b*	*c*	*d*	*e*	*f*	ref
amarantite	$[Fe_4O_2(SO_4)_4]$	131.9	96.3	131.9	83.7	1.892	1.969	1.929	3.440[b]	3.526[b]	2.93	5
leucophosphite	$[Fe_4(OH)_2(PO_4)_4(H_2O)_2]$	124.05[b]	91.82[b]	122.9[b]	88.2[b]	2.150	2.175	2.152[b]	3.820[b]	3.778[b]	3.108[b]	6
1	$[Fe_4O_2(BICOH)_2(BICO)_2(O_2CPh)_4]^{2+}$	119.0 (6)	95.7 (5)	136.8 (6)	84.3 (5)	1.884 (9)	1.98 (1)	1.94 (1)	3.29 (1)	3.59 (1)	2.90 (1)	*c*
2	$[Fe_4O_2(O_2CCF_3)_8(H_2O)_6]$	133.9 (2)	96.5 (2)	129.5 (2)	82.9 (2)	1.842 (4)	1.961 (3)	1.936 (3)	3.476 (2)	3.436 (3)	2.915 (3)	7
7	$\{Fe_4O_2\}$ core in $[Fe_8O_2(OH)_{12}(TACN)_6]^{8+}$	128.7 (3)	96.8 (4)	128.7 (1)	83.2 (5)	1.859 (9)	1.968 (18)	1.961 (5)	3.444 (12)	3.425 (6)	2.939 (4)	15
3	$[Fe_4O_2(O_2CPh)_7(H_2B(pz)_2)_2]^-$	125.1 (5)	93.5 (3)	133.6 (5)	85.4 (3)	1.822 (7)	1.955 (8)	1.895 (7)	3.326 (2)	3.488 (2)	2.829 (4)	8
		125.9 (5)	94.5 (3)	134.1 (5)	85.6 (3)	1.854 (8)	1.967 (8)	1.917 (7)	3.330 (2)	3.500 (2)		

[a] See Figure 3 for labels used to identify bond lengths and angles. [b] Calculated by using the data presented in the original references. [c] This work.

Table V. Visible Spectroscopic Absorptions of Compounds Containing the $\{Fe_4O_2\}$, $\{Fe_3O\}$, or $\{Fe_2O\}$ Iron(III) Oxo Core

compd	λ_{max},[a] nm (ϵ_{Fe}, M^{-1} cm^{-1})	ref
$[Fe_4O_2(BICOH)_2(BICO)_2(O_2CPh)_4]Cl_2$ (**1**)	575 (sh), 476 (sh)	*b*
$(Et_4N)[Fe_4O_2(O_2CPh)_7(H_2B(pz)_2)_2]$ (**3**)	565 (sh, 75), 467 (470)	8
amarantite, $\{Fe_4O_2\}$ core	500, 442, 434, 424	37
leucophosphite, $\{Fe_4(OH)_2\}$ core	538, 441.5, 428	37
$[Fe_2O(O_2CPh)_2(HB(pz)_2)_2]$	490 (430), 455 (480)	16b
$[Fe_3O(TIEO)_2(O_2CPh)_2]Cl_3$	492 (sh)	20

[a] sh = shoulder. [b] This work.

(31) Gözen, S.; Peters, R.; Owston, P. G.; Tasker, P. A. *J. Chem. Soc., Chem. Commun.* **1980**, *1199*–1201.
(32) Lippard, S. J.; Schugar, H. L.; Walling, C. *Inorg. Chem.* **1967**, *6*, 1825–1831.
(33) Gorun, S. M., Ph.D. Thesis, Massachusetts Institute of Technology, Cambridge, MA, 1986. The room-temperature (296.4 K) magnetic moment of $[Fe(TICO\text{-}CH_3)_2](ClO_4)_3$ is 2.8 μ_B.
(34) Sinn, E.; Sim, G.; Dose, E. V.; Tweedle, M. F.; Wilson, L. F. *J. Am. Chem. Soc.* **1978**, *100*, 3375–3390.
(35) Gorun, S. M.; Papaefthymiou, G. C.; Frankel, R. B.; Lippard, S. J. *J. Am. Chem. Soc.* **1987**, *109*, 3337–3348.

in various compounds. The Fe_4 rhombus is defined by *d*, *e*, and *f*, the dimer by *a*, *c*, and *d* or α, the kernel by *b*, *c*, and either β or δ, and an $\{Fe_3O\}$ trimer subset by *a*–*f* and α–γ.

Table IV summarizes geometrical features of selected compounds having $\{Fe_4O_2\}^{8+}$ or $\{Fe_4(OH)_2\}^{10+}$ cores, from which may be drawn several general observations. The intradimer Fe–O–Fe angle, α, varies appreciably, encompassing the narrower 118–126° range observed in binuclear $\{Fe_2O\}^{4+}$ cores.[17] This variation may be due to different steric requirements for bridging groups spanning the rhombus edge *d*, PO_4^{3-} in leucophosphite, SO_4^{2-} in amarantite (one on each side), two benzoate bridges along *d* and one $BICO^-$ ligand along *e* in **1**, one μ-CF_3COO^- along each side in **2**, and two benzoate bridges along *d* and one along *e* in **3**. The angle α alone clearly cannot be used to distinguish between μ_3-oxo and μ_3-hydroxo groups. The sum of angles, $\alpha + \beta + \gamma$, around the μ_3-oxo group is 360° in amarantite and in **2**; i.e., the oxo atom is in the plane of the Fe_4 rhombus. In **1**, the angle sum is only ~352°, with the μ_3-oxo atom being displaced 0.32 Å from the best plane through the four iron atoms. The sum of the Fe–O–Fe angles around the μ_3-OH oxygen atom in leucophosphite is 338.8°, comparable with the value of 328.4° expected for pure sp^3 hybridization. The hydroxide oxygen atom is displaced by 0.57 Å from the best Fe_4 plane.

The kernel Fe–O(oxo) distances *b* and *c* are remarkably constant and significantly shorter than the corresponding Fe–O(hydroxo) distances. The Fe–O intradimer distance *c* is consistently shorter than one of the interdimer distances, *b*, but longer than the other one, *a*. This difference is evident for both μ_3-oxo and μ_3-hydroxo bridged complexes and may be used to define "the dimer" as the unit having the shortest two Fe–O bonds. For example, if we refer to Figure 3 and the amarantite and leucophosphite structures, a second choice for the dimeric binuclear unit could be Fe1 and Fe2′, but the criterion $b > c$ establishes, in accord with the crystal structure, the unique half of the tetranuclear unit. Deviations from idealized geometry thus seem to be remarkably self-consistent within the series of planar Fe_4 compounds listed in Table IV. One exception is the significantly smaller value of *f* for compound **3**, which is unique in having a carboxylate bridge across Fe2 and Fe2′ and a decidedly nonplanar Fe_4 core.

The angle γ varies significantly, even within the μ_3-oxo series, since this angle is spanned by groups that provide interdimer linkages. The inter- and intradimer Fe···Fe distances *e* and *d* show similar variations.

Surprisingly, β, δ, and (except for **3**) *f* are almost independent of interdimer linkage type, again reflecting the rigidity of the kernel. Only when the μ_3-oxo group is protonated does the kernel expand, but the major change is to increase *a*, which becomes equal to *c*. The rigidity of the kernel is maintained even in **1**, where the μ_3-oxo atoms lie out of the Fe_4 plane and the plane of the kernel makes a dihedral angle of 14° with the Fe_4 plane by rotation around the Fe2–Fe2′ axis. These observations provide useful criteria for establishing the existence of a μ_3-OH group, especially for large crystal structures in which protons may be difficult to locate from electron density difference Fourier maps.

The metrical parameters of the $\{Fe_4O_2\}$ core in the octanuclear complex **7**, also compare remarkably well with the other compounds in Table IV. The oxygen atoms are located 0.3 Å above and 0.2 Å below the least-squares plane defined by the four iron atoms, which are within 0.009 Å of their best mean plane. The four kernel atoms are within 0.018 Å of the least-squares plane they define, which in turn makes an angle of 11.3° with the Fe_4 plane. The corresponding value in **1** is 14°. The sums of angles around the μ_3-oxo oxygen atoms are 352.4 and 356.2°.

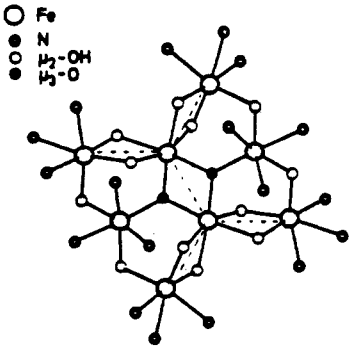

7

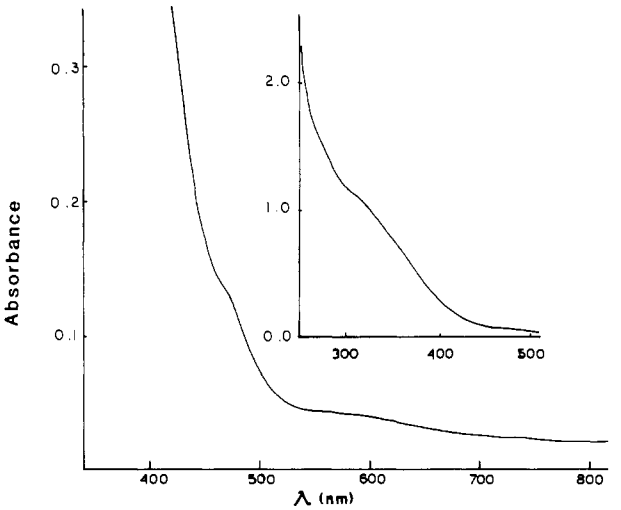

Figure 4. UV–visible spectrum of a solution of **1** in CH_2Cl_2, showing an expanded version in the inset.

The kernel for planar compounds listed in Table IV is constant, despite the presence of very different intra- and interdimer bridges. The central $\{Fe_2O_2\}$ subset of the $\{Fe_4O_2\}$ core thus appears to be a structural invariant, one likely to be encountered in other compounds containing $\{Fe_4O_2\}$ units with μ_3-oxo, but not μ_3-hydroxo, bridges.

Spectroscopic, Magnetic, and Mössbauer Properties. The infrared spectrum of **1** contains the well-known absorptions of H_2O (3400 cm^{-1}) and bridging benzoate groups (1600–1560, 1405, 730 cm^{-1}). A strong band at 975 cm^{-1} occurs in the region where metal–alkoxide ν_{C-O} stretches occur[36] and is therefore tentatively assigned to this vibration. An unassigned feature at 860 cm^{-1} may be associated with the $\{Fe_4O_2\}^{8+}$ core, but further studies, including ^{18}O substitution and Raman spectroscopy, are required to obtain definitive assignments of the vibrational modes of this tetranuclear unit in **1**, **3**, and related complexes.

The solution optical spectrum of **1** is presented in Figure 4. Two shoulders located at 476 and 575 nm are not found in compounds containing the binuclear $\{Fe_2O\}^{4+}$ [17b] or trinuclear $\{Fe_3O\}^{7+}$ [20] cores with bridging benzoate groups but match quite well the optical transitions in $[Fe_4O_2(O_2CPh)_7(H_2B(pz)_2)_2]^-$ (**3**) (Table V). The molar extinction coefficients of these bands in **1**, ~10^2 cm^{-1} M_{Fe}^{-1}, are of the same order of magnitude as reported for **3**, as well as (μ-oxo)bis(μ-carboxylato)diiron(III) complexes.[11,17] Table V also lists the visible absorption bands of amarantite and leucophosphite in the solid state, the assignments of which are discussed elsewhere.[37] Unfortunately, it is not straightforward to compare these values with solution spectral results for **1** and **3**, especially since the optical transitions for the minerals have been associated with solid-state effects. On the basis of the limited information available, however, it would appear that solution optical absorptions at ~465–475 and 565–575 nm may provide a useful tool for discriminating between the $\{Fe_4O_2\}^{8+}$ unit and its $\{Fe_3O\}^{7+}$ and $\{Fe_2O\}^{4+}$ subsets.

The solid-state effective magnetic moment of **1** decreases from 2.4 μ_B per iron at 290 K to 1.2 μ_B at 80 K and reaches a value of 0.4 μ_B at 4 K, consistent with a diamagnetic ground state. The residual paramagnetism obeys the Curie law below 20 K and is due to a few percent of paramagnetic impurity, probably $FeCl_3$.[33]

(36) Nakamoto, K. *Infrared and Raman Spectra of Inorganic and Coordination Compounds*, 3rd ed.; Wiley: New York, 1978, pp 230.
(37) Rossman, G. R. *Am. Mineral.* **1976**, *61*, 933–938.

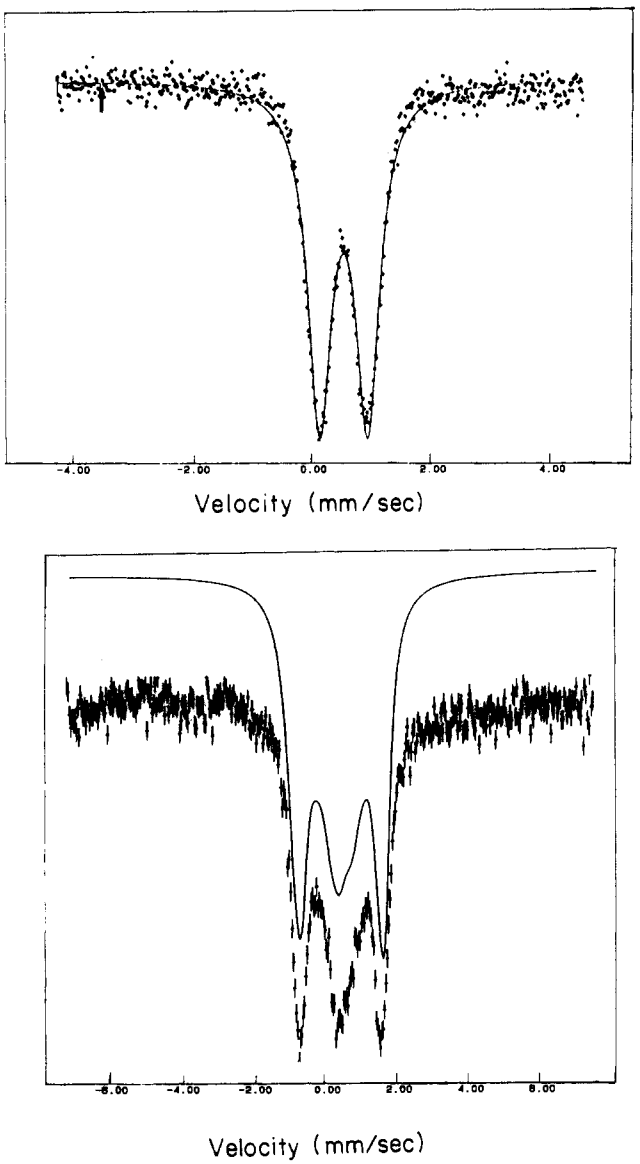

Figure 5. Zero-field (top) and 60 kOe (bottom) Mössbauer spectra of solid **1** at 4.2 K. Parameters used to simulate the experimental points are given in the text; the line width (Γ) is 0.48 mm/s.

The diamagnetic ground state implies antiferromagnetic exchange coupling among the four high-spin ferric ($S = {}^5/_2$) centers to produce a total spin $S_T = 0$. Similar behavior occurs for the $\{Fe_4O_2\}^{8+}$ core in **3**,[8] as well as the tetranuclear iron(III) centers in **4**[9] and **5**.[10] Magnetic exchange coupling constants have been evaluated for compound **4**, $Na_6[Fe_4L_2O_2(CO_3)_2]$, J being -63.4 cm^{-1} for the "intradimer" oxo/carbonato-bridged pairwise interaction of iron(III) centers.[9] A second J value of -11.2 cm^{-1} characterizes an additional "interdimer" exchange interaction between pairs of $\{Fe_2O(CO_3)\}$ units within the tetranuclear cluster. The J value of -63.4 cm^{-1} seems low for a (μ-oxo)diiron(III) center,[17] but there is apparently some ambiguity about the chemical composition of **4** and it seems possible that the μ-oxo group might have an H^+ ion near it.[9] Such an interaction would certainly attenuate the magnetic exchange coupling.[28d] The room-temperature effective magnetic moment of **1** compares favorably with the value of 2.5 μ_B obtained for amarantite.[37] Leucophosphite has a room-temperature effective moment of 5.1 μ_B which, although less than the 5.92 μ_B spin-only value for isolated high-spin ferric salts, again reflects the lesser ability of hydroxo versus oxo bridges to mediate strong antiferromagnetic exchange interactions in polyiron(III) clusters.[28d] A more thorough theoretical analysis of the magnetic properties of **1** and other tetranuclear iron(III) complexes is currently being undertaken.

Mössbauer spectra of solid **1** at zero-field and 60 kOe are presented in Figure 5. The isomer shift of 0.5 ± 0.03 mm/s is of the expected magnitude for high-spin iron(III)[38] and is close to the values reported for **2**[30] and **3**.[8] The magnetic Mössbauer spectrum confirms the presence of a diamagnetic ground state, $S_T = 0$, in accord with the magnetic susceptibility measurements. The quadrupole splitting value of 0.81 mm/s is outside the 1.5–2.0 mm/s range observed for (μ-oxo)diiron(III) complexes[17] but larger than the 0.4–0.7 mm/s range observed for basic iron carboxylates.[39] In the most closely related complexes **2** and **3**, ΔE_Q is 0.78 mm/s (average over two sites) at 80 K and 1.21 mm/s at 4.2 K, respectively. Although the inequivalent iron subsites could be resolved in Mössbauer spectra of **2**, such was not the case for compounds **1** and **3**.

Conclusions

A new bis(μ_3-oxo) tetranuclear iron(III) complex has been synthesized and characterized by X-ray crystallography, magnetic measurements, and optical, vibrational, and Mössbauer spectroscopy. It has spectroscopic and structural features in commmon with other known complexes containing the $\{Fe_4O_2\}^{8+}$ core, but different structural, vibrational, optical, magnetic, and Mössbauer properties when compared with those of known complexes containing either the $\{Fe_2O\}^{4+}$ or the $\{Fe_3O\}^{7+}$ cores. These similarities and differences should help, in particular, to distinguish this core in other minerals, synthetic complexes, or metalloproteins that lack structural data and to improve our understanding of the iron oxo complexes in general.

The ligands involved in coordinating the tetranuclear iron core, imidazole, carboxylate anions, and triply-bridging oxygen atoms, occur in biology and point toward the possibility of forming such complexes in vivo. This view is supported by the presence of $\{Fe_4O_2\}$ type units in minerals. The objective of synthesizing (μ-oxo)bis(μ-carboxylato)diiron(III) complexes with imidazole ligands has been reached, but in the absence of a protective protein environment, the open coordination sites have been filled by aggregation. This aggregation phenomenon will have to be overcome in future synthetic efforts to obtain functional Hr analogues. The result in the present case is the formation of a tetranuclear iron oxo cluster, but this analysis has no mechanistic implications. Initial formation of a tetranuclear or other oligomeric iron oxo aggregate before the addition of BICOH cannot be excluded. Further synthetic efforts are required to delineate the role of polydentate ligands in controlling the degree of aggregation and chemistry of this interesting, new, and growing class of polyiron oxo complexes.

Acknowledgment. This work was supported by National Institutes of Health Research Grant GM32134 from the National Institute of General Medical Sciences. We are grateful to Drs. G. C. Papaefthymiou and R. B. Frankel of the Francis Bitter National Magnet Laboratory for Mössbauer spectra.

Registry No. **1**, 111410-35-6; BICOH, 67319-03-3; $(Et_4N)_2[Fe_2OCl_6]$, 87495-23-6.

Supplementary Material Available: Tables containing thermal parameters for non-hydrogen atoms (Table S1) and hydrogen atom positional and thermal parameters (Table S2) for compound **1** (2 pages); a table containing observed and calculated structure factors (Table S3) for compound **1** (54 pages). Ordering information is given on any current masthead page.

(38) (a) Greenwood, N. N.; Gibb, T. C. *Mössbauer Spectroscopy*; Chapman and Hall: London, 1971; pp 148–164. (b) Murray, K. S. *Coord. Chem. Rev.* **1974**, *12*, 1–35.

(39) Long, G. J.; Robinson, W. T.; Tappmeyer, W. P.; Bridges, D. L. *J. Chem. Soc., Dalton Trans.* **1973**, 573–579.